

# Imaging of Paranasal Sinuses and Anterior Skull Base and Relevant Anatomic Variations

Estushi Iida, MD<sup>a</sup>, Yoshimi Anzai, MD, MPH<sup>b,\*</sup>

## KEY WORDS

- Anterior skull base • Sinonasal cavity • Computed tomography • MR imaging • Neoplasm
- Inflammatory disease

## KEY POINTS

- The anterior skull base (ASB) is the boundary between the anterior cranial fossa and sinonasal cavities and orbits.
- In addition to the intrinsic ASB lesions, sinonasal lesions extend superiorly to involve ASB and also intracranial lesions extend to ASB.
- CT and MRI play a complementary role in evaluating and characterizing ASB pathologies.
- Radiologists should be familiar with the detailed anatomy, identify dangerous anatomical variations, provide appropriate differential diagnosis, and assess the extent of the lesion for optimal treatment planning.

## INTRODUCTION

The anterior skull base (ASB) is the boundary between the anterior cranial fossa and sinonasal cavities and orbit, consisting of the frontal bone, ethmoid bone, and sphenoid bone. ASB pathologic conditions can be divided into 3 major categories: (1) sinonasal lesions extending cranially, (2) intrinsic ASB lesions, and (3) intracranial lesions involving the ASB.

Computed tomography (CT) and MR imaging play important roles in providing a diagnosis or differential diagnosis, assessing the extent of ASB lesions, and guiding treatment decisions and surgical approach.

The recent advances in the endoscopic sinusal and skull base surgery allow a minimally invasive surgery for a wide variety of pathologic

conditions, including congenital and inflammatory diseases, and benign and malignant neoplasms. Because these endoscopic procedures use sinusal cavity as surgical corridors, the preoperative evaluation of sinusal cavity is critical to facilitate the safe access to a target lesion. Radiologists should be aware of sinusal anatomic variants that can create impediments to surgical access, decrease surgical field orientation, and increase risk of vascular or cranial nerve injury during the surgery.

This article briefly addresses CT and MR imaging techniques and reviews the ASB anatomy. In particular, it describes the sinusal anatomy and its variants pertinent to endoscopic approach to the skull base. Clinical and imaging findings of ASB pathologic conditions are also discussed.

<sup>a</sup> Department of Radiology, Yamaguchi University Graduate School of Medicine, 1-1-1 Minami-Kogushi, Ube, Yamaguchi 755-8505, Japan; <sup>b</sup> Department of Radiology, University of Utah Health Sciences Center, 30 North, 1900 East #1A071, Salt Lake City, UT 84132-2140, USA

\* Corresponding author.

E-mail address: Yoshimi.Anzai@hsc.utah.edu

## IMAGING TECHNIQUE

CT and MR imaging play a complementary role in characterization and determination of the extent of the ASB pathologic condition. CT provides better detail of the bony anatomy and the extent of pneumatization. It also clearly demonstrates presence of calcification, bone remodeling, and destruction, and characterizes fibro-osseous pathologic conditions. MR imaging offers much superior contrast resolution and is useful in delineating the extent of disease and characterizing soft tissue pathologic conditions.

### *Computed Tomography*

Thin axial CT images should be acquired using the multirow detector CT with 0.5 to 0.625 mm collimation to obtain sufficient information about osseous anatomy and pathologic changes in the skull base and sinonasal cavity. Images are reconstructed to axial, coronal, and sagittal planes with high-resolution bone and soft-tissue algorithms.

Noncontrast-enhanced CT is usually sufficient for assessment of fibro-osseous lesion. Contrast-enhanced CT should be considered if there is a clinical concern for extrasinus extension of infection, abscess, venous thrombosis, or neoplasm.

### *MR Imaging*

MR sequences should include T1-weighted images (T1WIs) and T2-weighted images (T2WIs), and contrast-enhanced fat-saturated (CEFS)-T1WI in axial and coronal planes covering the sinusal cavity to intracranial structures. Thin-slice thickness (2 mm or less) is preferred. T1WI is useful to detect subtle abnormal findings in bone

marrow and adipose tissue as well as detection of proteinous secretion, hemorrhage, and melanin. A T1WI with CEFS-T1WI is necessary to delineate an enhancing lesion from intrinsic T1WI hyperintensity due to fat containing lesions. T2WI is useful for distinguishing isointense neoplasm from hyperintense obstructed sinus secretion. Fat suppression allows better contrast between tumor and sinonasal secretion. Coronal CEFS-T1WI is valuable for assessment of perineural spread through the ASB. Sagittal images allow clear delineation of the craniocaudal extension of the ASB lesions.

## NORMAL ANATOMY OF THE ANTERIOR SKULL BASE

The ABS consists of the frontal bone (orbital plate), ethmoid bone (cribriform plate, lateral lamella, and fovea ethmoidalis), and sphenoid bone (planum sphenoidale and lesser wing) (**Fig. 1**). The superior surface of the orbital plate forms the lateral parts of the ASB. The planum ethmoidal and sphenoidale are posterior to the cribriform plate, forming the roof of the ethmoid and sphenoid sinuses, respectively. The planum sphenoidale leads laterally to the lesser wing of the sphenoid bone and posteriorly to the prechiasmatic groove and the tuberculum sellae. The anterior clinoid process forms the posteromedial part of the lesser wing. The posterior edge of the lesser wing is the posterior boundary of the anterior cranial fossa.

The crista galli is a bony protuberance in the midline of the cribriform plate. The foramen cecum is between the frontal bone anteriorly and the crista galli posteriorly, and has a variable size. It transmits emissary veins from the nasal mucosa

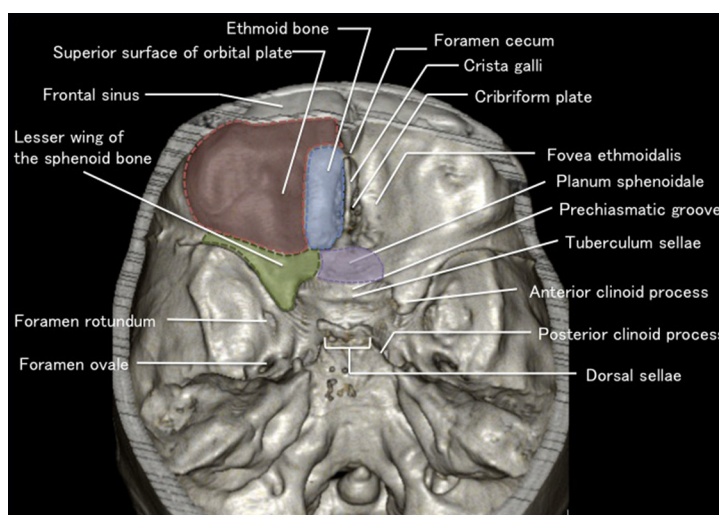


**Fig. 1.** Anatomy of the anterior skull base. Volume rendering CT image of the skull base demonstrates an overview of the anterior cranial fossa.

to the superior sagittal sinus but often presents as a vestigial fibrous tract.

The cribriform plate and the lateral lamella form the olfactory fossa where olfactory bulb is located. The fovea ethmoidalis, which forms the roof of the ethmoid cells connects the lateral lamella with the orbital plate of the frontal bone (Fig. 2). These ethmoidal components are thin and prone to injury, which may result in cerebrospinal fluid (CSF) leak. Increased depth of the olfactory fossa is associated with increased risk of injury during surgery. Keros classification is used to classify the depth of olfactory fossa and the height of the lateral lamella for the preoperative evaluation as follow: 1 to 3 mm, type I; 4 to 7 mm, type II; and 8 to 16 mm, type III.<sup>1</sup> The Keros type III has the higher risk of bone erosion or CSF leak.

## NORMAL AND VARIANT ANATOMY OF THE SINONASAL CAVITY

Because the nasal cavity is the primary corridor to the skull base, it is pertinent to evaluate the anatomy of nasal cavity for the endoscopic approach. The nasal septum and the 3 (inferior, middle, and superior) turbinates separate the nasal cavity into 8 air chambers (the inferior, middle, and superior meatus ethmoidal, and the sphenooethmoidal recesses in each side). The vertical and basal lamellae of the middle turbinate insert into the

cribriform plate and lamina papyracea, respectively, which are at risk of injury during surgery (see Fig. 2). The uncinate process arises from the inferior turbinate and variably inserts into the lamina papyracea or the cribriform plate. Nasal septum deviation and concha bullosa, pneumatization of the middle turbinate occasionally limit the access to the posterior nasal cavity or determine the side of access.

Sphenoid sinus is adjacent to many vital structures, including the optic nerves, the internal carotid arteries, the cavernous sinuses, and the pituitary gland. The sphenoid ostium opens to the sphenoethmoid recess at the superior part of the anterior sphenoid sinus wall (Fig. 3). The pneumatized nasal septum can limit access to the ostium (see Fig. 3).

The sphenoid sinus pneumatization is significantly variable in individuals and classified into 4 types (conchal, presellar, incomplete sellar, and complete sellar) based on the anteroposterior dimension (Fig. 4).<sup>2</sup> The complete sellar type is the most frequent and favorable for the transsphenoidal approach, whereas conchal and presellar types need drilling of bone to access to the floor of the sella.<sup>2</sup>

The sphenoid pneumatization can reach superiorly to the clinoid processes, laterally to the greater wing (forming the lateral recess of the sphenoid sinus), and inferolaterally to the

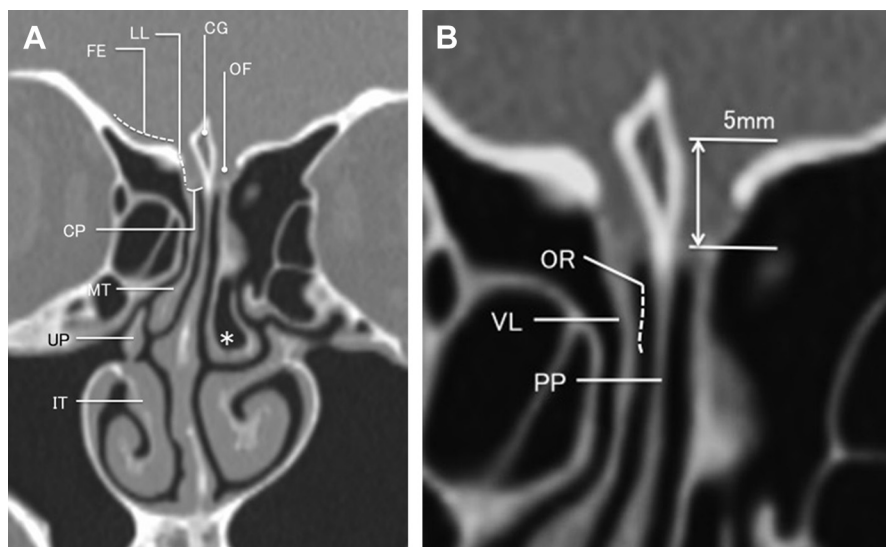


**Fig. 2.** Anatomy of the median anterior skull base. (A) Coronal CT. (B) Magnification of A. (A) The olfactory fossa (OF) is formed by the cribriform plate (CP) and lateral lamella (LL). The fovea ethmoidalis (FE) is the ethmoid roof. CG, crista galli; IT, inferior turbinate; MT, middle turbinate; UP, uncinate process. (B) The vertical lamella (VL) of the middle turbinate inserts to the cribriform plate forming the olfactory recess (OR) with the perpendicular plate (PP) of the ethmoid bone (B). The depth of the olfactory recess has a close relation with the risk of the injury to the cribriform plate. Left concha bullosa (pneumatized middle turbinate) is present (\*).

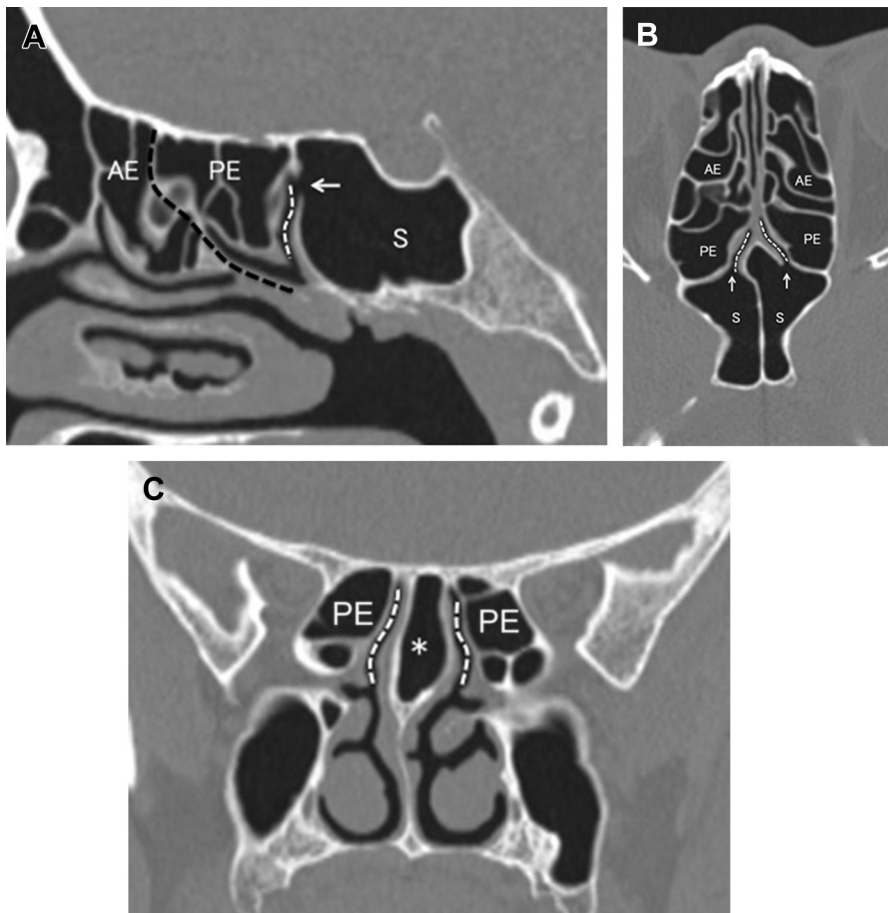


**Fig. 3.** CT anatomy of the ethmoid and sphenoid sinuses. (A) Sagittal CT. (B) Axial CT. (C) Coronal CT. Sphenoid ostia (arrows) locate at the superomedial part of the anterior walls of the sphenoid sinuses leading to sphenoethmoidal recesses (white dashed lines). The sphenovomerine bulla (asterisk in C) is present. The basal lamella of middle turbinate (black dashed line in A) divides ethmoid sinus into anterior and posterior ethmoid cells. AE, anterior ethmoid; PE posterior ethmoid; S(Sphenoid), sinuses.

pterygoid process (**Fig. 5**). Excessive pneumatization provides natural corridors for off-midline skull base lesions, although it can also increase the risk of neurovascular injury, secondary to protrusion and dehiscence of neurovascular canals (optic canal, carotid canal, pterygoid canal, and foramen rotundum).<sup>2</sup> Also, the intersphenoid and accessory septa potentially increase surgical risk if they insert to vital structures such as the carotid canal (see **Fig. 5**).<sup>2,3</sup>

The ethmoid sinus is divided into the anterior and posterior ethmoidal cells by the basal lamella of the middle turbinate (see **Fig. 3**). The agger nasi cell (the most anterior ethmoid air cell) and the ethmoid bulla (the largest anterior ethmoid air cell) are reliable anatomic landmarks for endoscopic surgery.

The anterior ethmoid canal, which houses the anterior ethmoid artery, is also an important

surgical landmark. It is usually embedded in the ethmoidal roof but occasionally traverses the ethmoid air cells in a mesentery below the roof, which increases the risk of injury (**Fig. 6**).<sup>4</sup>

The supraorbital ethmoid air cell is an anterior ethmoid air cell located posterolateral to the frontal sinus and may be mistaken for the frontal cell (**Fig. 7**). A bony septum between the frontal and anterior ethmoid sinuses on axial and sagittal CT suggests the presence of a supraorbital ethmoid air cell. It can impose a risk of orbital and ASB injury during endoscopic surgery. Violating the supraorbital air cell during anterior cranial fossa approach to orbit increases the risk of surgical site infection.<sup>5</sup>

The Onodi cell, also known as the sphenoethmoidal cell, is a variant of the posterior ethmoidal cell that extends superior and/or lateral to the sphenoid sinus (**Fig. 8**). It often extends into the

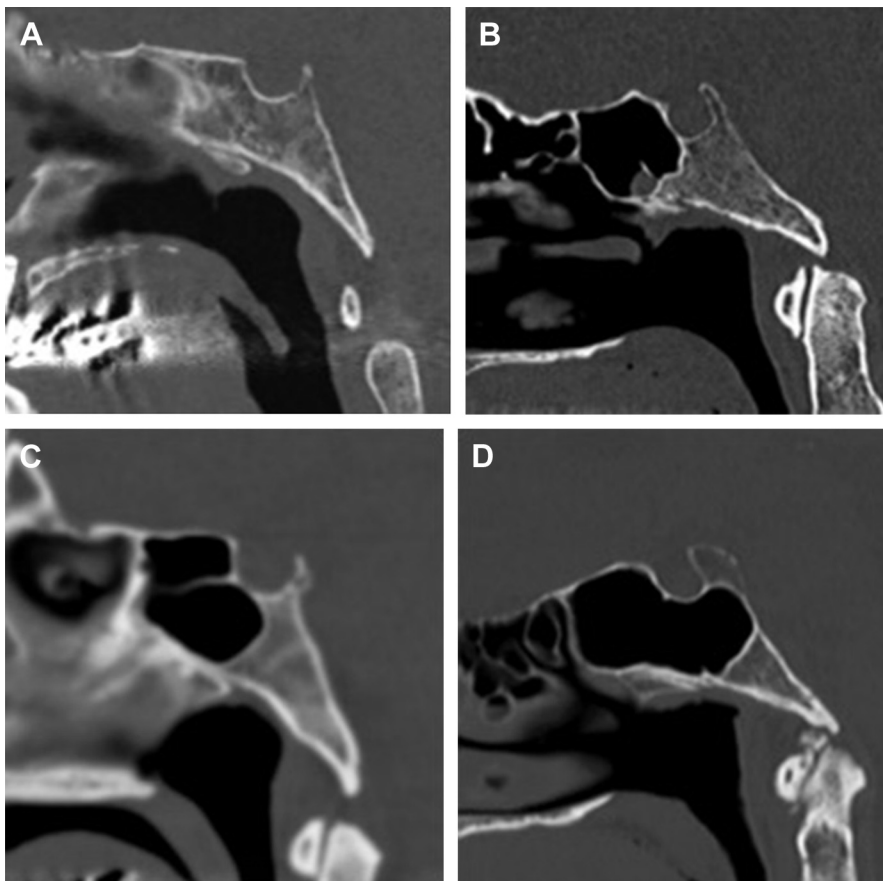


**Fig. 4.** Classification of sphenoid pneumatization on sagittal CT images. (A) Conchal type. (B) Presellar type. (C) Incomplete seller type. (D) Complete seller type.

anterior clinoid process, increasing risk of injury to the optic nerve and the internal carotid artery as well as CSF leakage.<sup>6</sup> Coronal CT images can directly demonstrate a horizontal septum between the Onodi cell and sphenoid sinus, whereas the sphenoid sinus septa only run in a vertical orientation.<sup>2,3,7</sup>

A dehiscence of the lamina papyracea increases the risk of orbital injury.<sup>3</sup> The anteroposterior diameter of the frontal sinus is related to maneuverability of the endoscopic instruments inside the sinus.<sup>8</sup>

#### ANTERIOR SKULL BASE PATHOLOGIC CONDITIONS

##### *Sinonasal Lesions Involving the Anterior Skull Base*

Both malignant and benign sinonasal diseases may involve the ASB. Extensive permeative bone destruction is associated with aggressive malignant neoplasms, whereas expansile osseous

remodeling suggests slow-growing lesions, such as low-grade malignancies, benign tumors, and mucoceles.

##### *Malignant sinonasal neoplasms*

Squamous cell carcinoma is the most common malignant neoplasm of the sinonasal cavity.<sup>9,10</sup> Other relatively common malignancies are adenocarcinoma, melanoma, and a variety of epithelial neoplasms with differing degrees of differentiation.<sup>10</sup>

**Malignant epithelial tumors (sinonasal carcinoma)** According to the World Health Organization histologic classification, sinonasal carcinomas are classified into 6 major types: squamous cell carcinoma, adenocarcinoma, salivary gland-type carcinoma, undifferentiated carcinoma, lymphoepithelial carcinoma, and neuroendocrine tumors.<sup>9</sup>

Squamous cell carcinoma frequently arises from maxillary sinus, whereas adenocarcinoma often

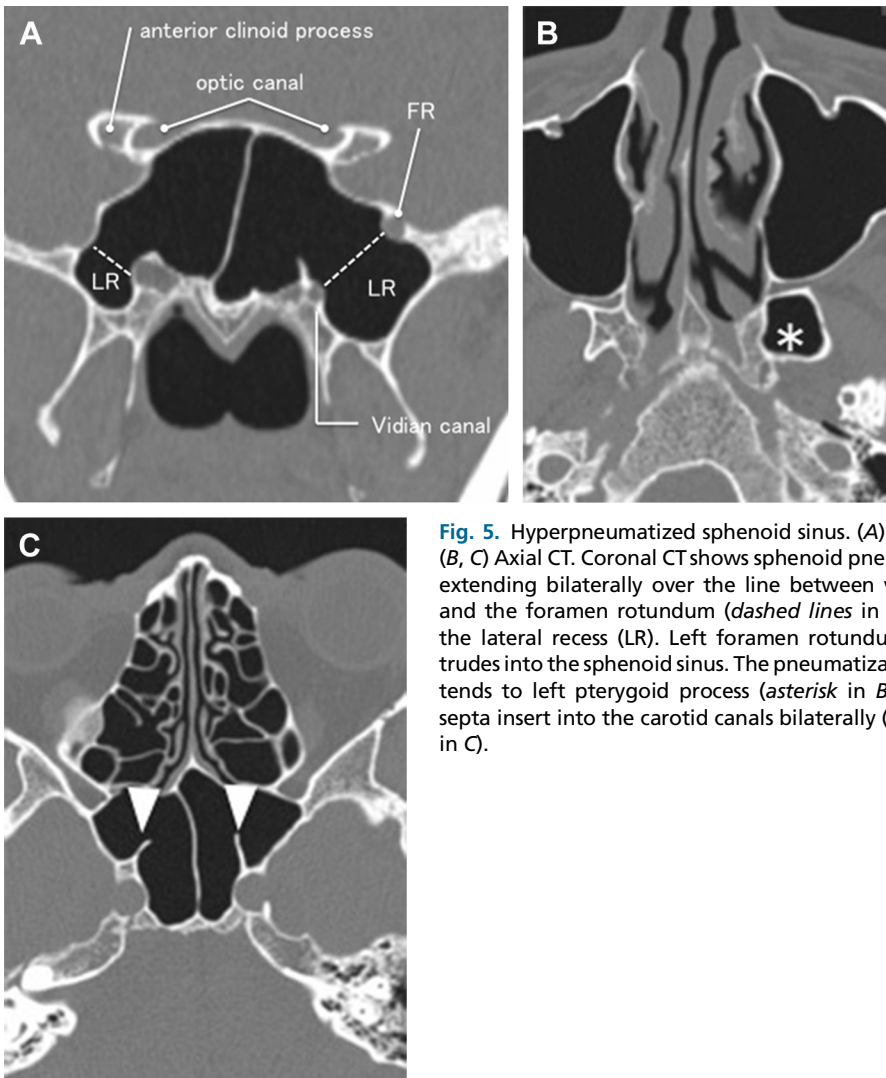


**Fig. 5.** Hyperpneumatized sphenoid sinus. (A) Coronal CT. (B, C) Axial CT. Coronal CT shows sphenoid pneumatization extending bilaterally over the line between vidian canal and the foramen rotundum (dashed lines in A), forming the lateral recess (LR). Left foramen rotundum (FR) protrudes into the sphenoid sinus. The pneumatization also extends to left pterygoid process (asterisk in B). Accessory septa insert into the carotid canals bilaterally (arrowheads in C).

originates from ethmoid sinus.<sup>9</sup> Sinonasal undifferentiated carcinoma originates from the nasal cavity and ethmoid sinus, and is associated with aggressive features with a rapidly progressive course.<sup>11</sup> Lymphoepithelial carcinoma, a rare tumor, is the counterpart of undifferentiated nasopharyngeal carcinoma, often arising from the

nasal cavity in Southeast Asian populations, and favorably responds to radiotherapy and radiochemotherapy.<sup>9</sup>

The tumor-nodes-metastasis (TNM) classification and staging system, based on the 7th edition of *AJCC Staging Manual* from the American Joint Committee on Cancer (AJCC),

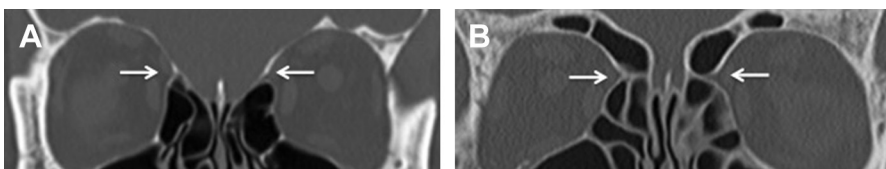


**Fig. 6.** Anterior ethmoid canal. The anterior ethmoid canal (arrow) courses in the ethmoidal roof to the lateral lamella (A). It occasionally traverses the ethmoid air cells in a mesentery below the roof, which increases the risk of injury to the anterior ethmoid artery (B).



**Fig. 7.** Supraorbital ethmoid air cell (SOE). (A) Axial CT. (B) Sagittal CT. The supraorbital ethmoid air cell can cause disorientation during endoscopic surgery resulting in inadvertent skull base injury. F, frontal sinus.

is available for carcinomas of the maxillary sinus, nasal cavity, and ethmoid sinus but not for those in the frontal and sphenoid sinuses due to their rarity.

Sinonasal tumor invasion to the skull base, dura, brain parenchyma, and orbit affects the tumor staging for both maxillary and nasoethmoid sinus cancer and is classified into tumor stage (T)-3, T4a, or T4b (**Table 1**), which translate to stage III, IVA, or IVB disease, respectively.<sup>12</sup>

CT provides detailed information about bone destruction. MR imaging is superior in distinguishing tumor from inflammatory changes and fluid retention (**Figs. 9–11**). Delineation of tumor margins is best accomplished by contrast-enhanced MR imaging sequences. Aggressive sinonasal carcinomas usually present a T2WI-intermediate signal with moderate enhancement, whereas sinonasal mucosa shows T2WI hyperintense signal with avid contrast enhancement. Secretion within obstructive sinus demonstrates variable signal intensities on both T1WI and T2WI sequences, depending on the protein content but lacks contrast enhancement. Low-grade adenocarcinoma and salivary gland-type carcinomas

can exhibit T2WI hyperintense signal due to abundant mucinous matrix and mimic benign tumors.<sup>13</sup>

Even with apparent bony erosion of the skull base or orbital wall, smooth bowing of a tumor interface suggests that the tumor is still limited by the periosteal layer of dura mater, orbital periosteum, or periorbital fascia.<sup>9,13,14</sup> MR imaging can demonstrate these structures as a hypointense hairline (see **Fig. 9**). In contrast, irregular or ill-defined margin is highly suggestive of tumor infiltration (see **Figs. 10 and 11**).<sup>13,15</sup> Nodular dural thickening and pial enhancement are highly suggestive of dural invasion (see **Fig. 10**).<sup>13–16</sup> Brain parenchymal or pial involvement causes vasogenic edema and parenchymal enhancement (see **Figs. 10 and 11**).<sup>13–15</sup>

**Esthesioneuroblastoma** Esthesioneuroblastoma, an uncommon tumor, arises from the olfactory epithelium in the upper third of the nasal cavity and frequently extends intracranially (**Fig. 12**).<sup>9,17</sup> Although not specific, marginal cysts adjacent to the intracranial tumor are characteristic imaging findings (**Fig. 13**).<sup>18,19</sup>

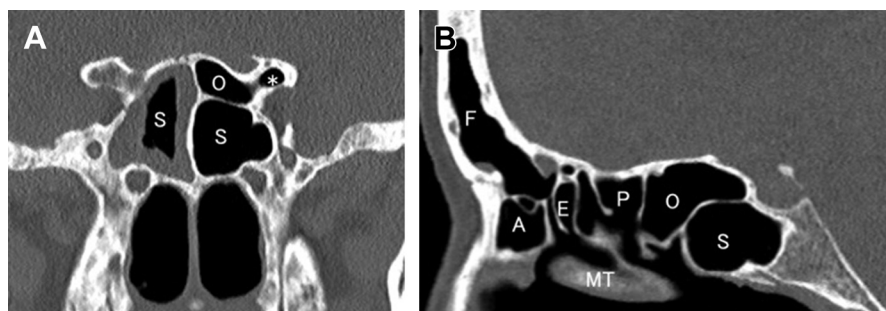


**Fig. 8.** Onodi cell (sphenoethmoidal cell) and pneumatized anterior clinoid process. (A) Coronal CT. (B) Sagittal CT. Coronal and sagittal CT images demonstrate left Onodi cell (O) above the left sphenoid sinus (S). Left pneumatized anterior clinoid process (asterisk in A) is also seen on coronal CT. Mucosal thickening presents in the right sphenoid sinus. A, agger nasi cell; E, ethmoid bulla; F, frontal sinus; MT, middle turbinate; P, posterior ethmoid cell.

**Table 1**  
Tumor staging of sinonasal carcinoma relating to skull base and orbital invasion

|   | Maxillary Carcinoma | Nasoethmoid Carcinoma |
|---|---------------------|-----------------------|
| <b>Skull base invasion</b>  |                     |                       |
| Cribiform plate   | T4a                 | T3                    |
| Minimal extension to anterior cranial fossa                         | —                   | T4a                   |
|   |                     |                       |
| Dura, brain, middle cranial fossa, clivus cranial nerve except CNV2 | T4b                 | T4b                   |
| <b>Orbital invasion</b>   |                     |                       |
| Medial wall/inferior wall   | T3                  | T3                    |
| Anterior orbital contents   | T4a                 | T4a                   |
| Orbital apex  | T4b                 | T4b                   |

The presence of intratumoral cysts, necrosis, and hemorrhage can affect the signal intensity and homogeneity of contrast enhancement.<sup>19,20</sup>

Similar to sinonasal carcinomas, presence of intracranial and orbital extension leads to worse outcome.<sup>21,22</sup> Kadish or modified Kadish classification is used for staging of esthesioneuroblastoma (**Box 1**).<sup>23–27</sup> In these staging systems, Kadish stage C, modified Kadish stage C-D (orbital and intracranial extension or metastases), is related to unfavorable prognosis.<sup>24,28–32</sup> The occurrence of cervical lymph node metastasis is 5% at the initial presentation, whereas the cumulative rate of late lymph node metastasis is 23.4%.<sup>24,33,34</sup>

Surgical resection with or without irradiation is generally an optimal treatment strategy. Chemotherapy is a valid option for patients presenting with high-grade pathologic condition, residual tumor, metastases, or recurrence.<sup>32</sup> Long-term follow-up is necessary because late recurrences are reported.<sup>22,33</sup>

**Lymphoma** Sinonasal lymphomas are mostly non-Hodgkin lymphomas and diffuse large B-cell

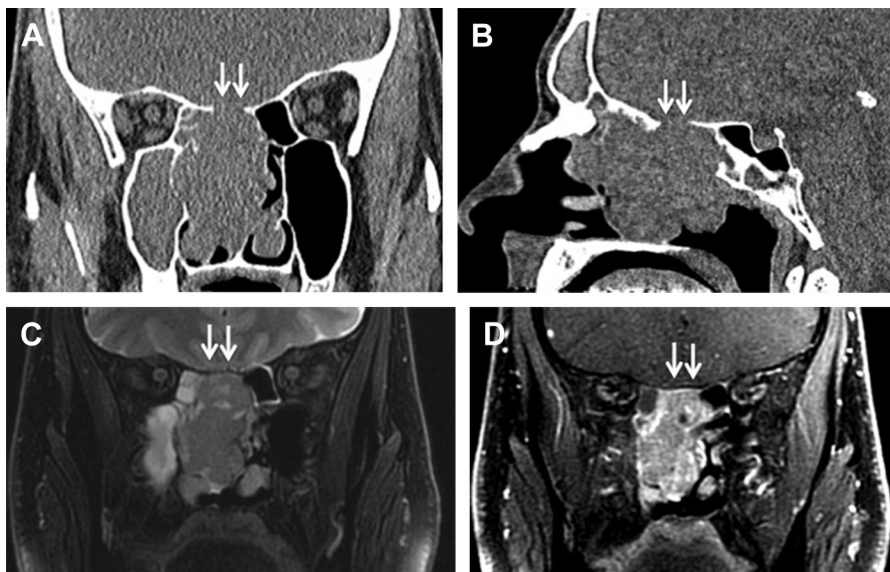


**Fig. 9.** Lymphoepithelial carcinoma. (A) Coronal CT. (B) Sagittal CT. (C) Coronal fat-saturated T2WI. (D) Coronal fat-saturated contrast-enhanced T1WI. Coronal and sagittal CT images show opacification in the right sinusal cavities with bone destruction of the planum ethmoidal (arrows in A, B), nasal septum, and ethmoid cells. (B) MR imaging demonstrates tumor limited in the nasal cavity. A thin hypointense line between the tumor and brain parenchyma (arrows in C, D) indicates intact periosteum. T2WI hyperintense signal within the right ethmoid and maxillary cells indicates obstructive sinusitis.

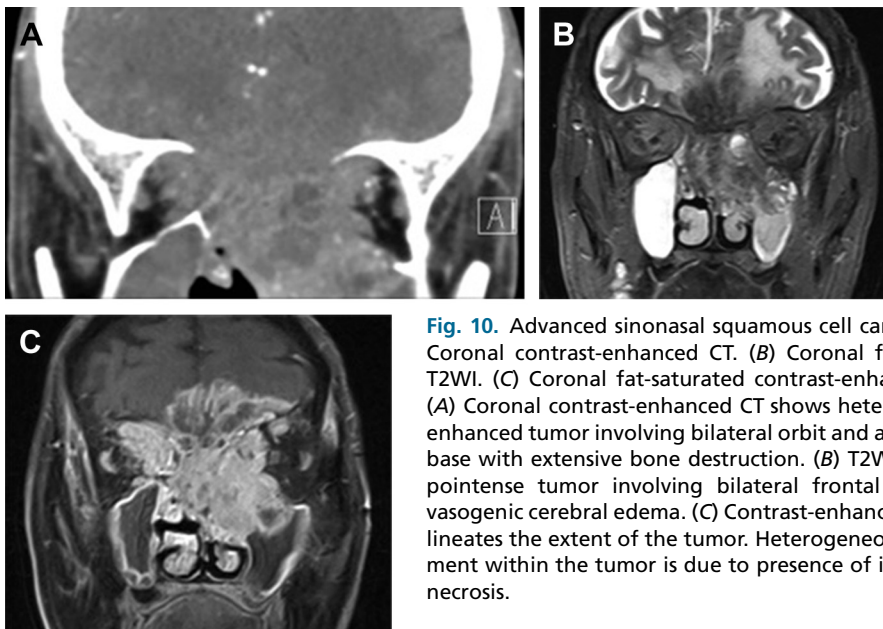


**Fig. 10.** Advanced sinonal squamous cell carcinoma. (A) Coronal contrast-enhanced CT. (B) Coronal fat-saturated T2WI. (C) Coronal fat-saturated contrast-enhanced T1WI. (A) Coronal contrast-enhanced CT shows heterogeneously enhanced tumor involving bilateral orbit and anterior skull base with extensive bone destruction. (B) T2WI shows hypointense tumor involving bilateral frontal lobes with vasogenic cerebral edema. (C) Contrast-enhanced T1WI delineates the extent of the tumor. Heterogeneous enhancement within the tumor is due to presence of intratumoral necrosis.

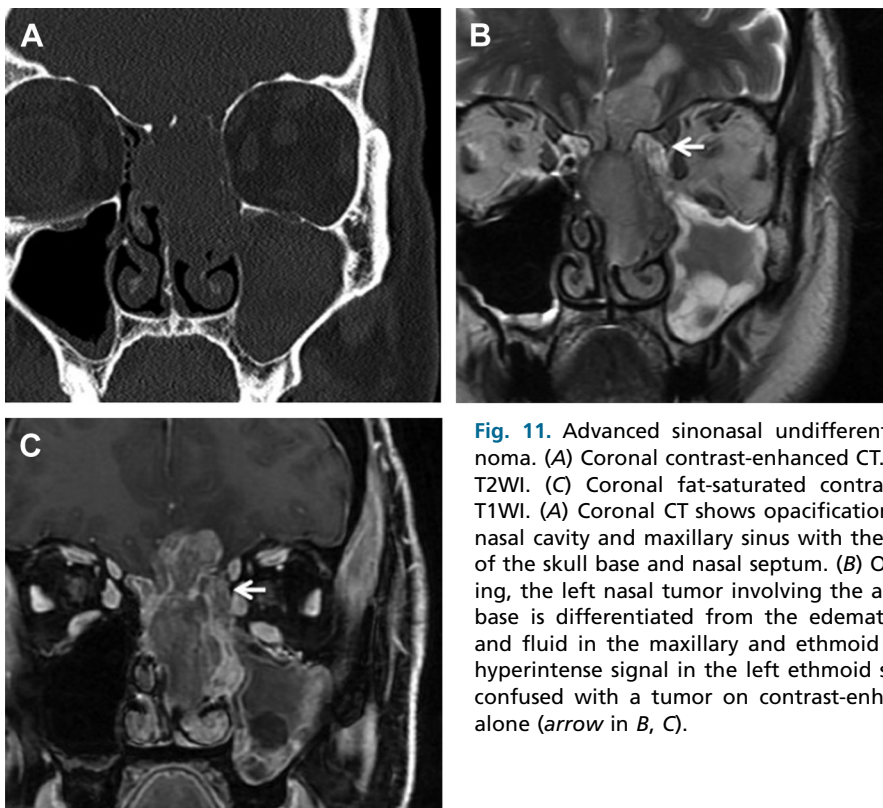


**Fig. 11.** Advanced sinonal undifferentiated carcinoma. (A) Coronal contrast-enhanced CT. (B) Coronal T2WI. (C) Coronal fat-saturated contrast-enhanced T1WI. (A) Coronal CT shows opacification in the left nasal cavity and maxillary sinus with the destruction of the skull base and nasal septum. (B) On MR imaging, the left nasal tumor involving the anterior skull base is differentiated from the edematous mucosa and fluid in the maxillary and ethmoid sinus. T2WI hyperintense signal in the left ethmoid sinus can be confused with a tumor on contrast-enhanced T1WI alone (arrow in B, C).

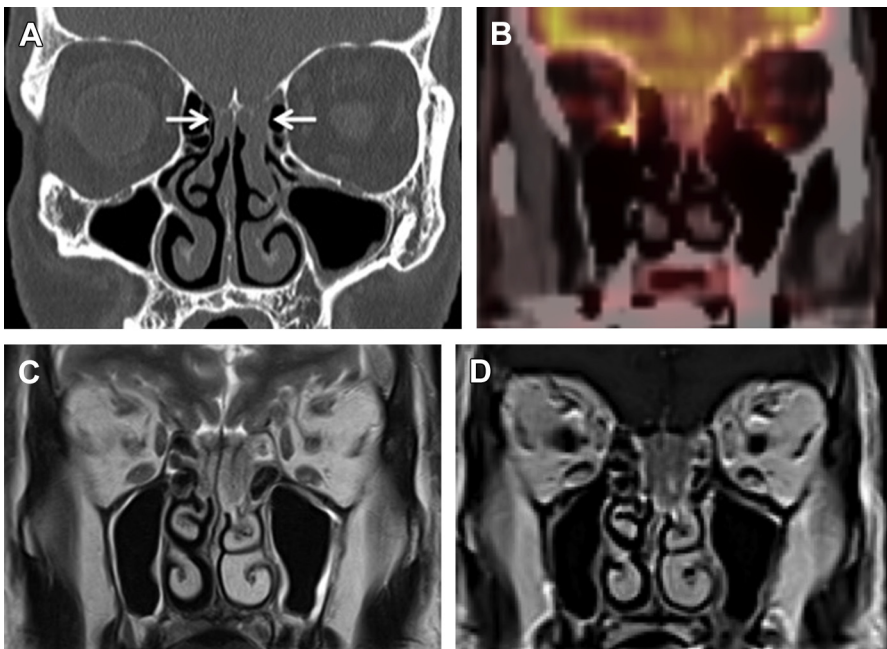


**Fig. 12.** Esthesioneuroblastoma. (A) Coronal CT. (B) Coronal fluorodeoxyglucose (FDG) PET/CT. (C) Coronal T2WI. (D) Coronal contrast-enhanced T1WI. Coronal CT shows subtle erosion of the cribriform plate with minimal mucosal thickening along the vertical lamella of middle turbinates (arrows in A). FDG PET/CT shows abnormal uptake corresponding to the lesion (B). The lesion shows intermediate T2WI signal intensity with moderate enhancement involving olfactory bulbs (C, D).

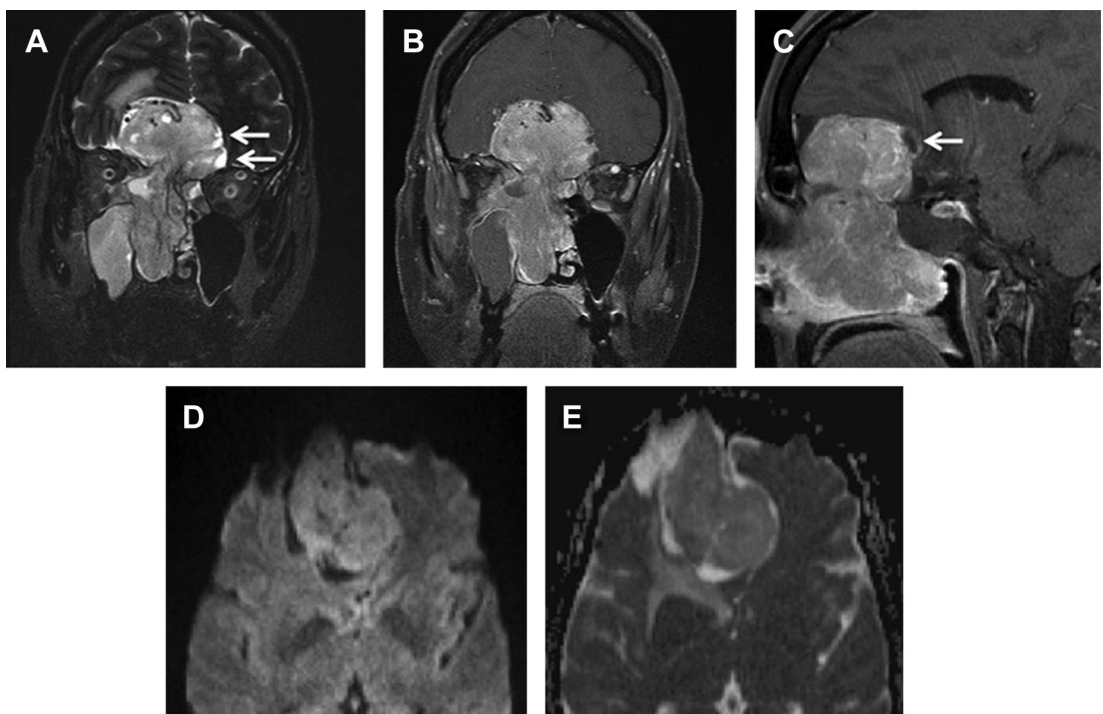


**Fig. 13.** Esthesioneuroblastoma with peritumoral cysts. (A) Coronal fat-saturated T2WI. (B) Coronal fat-saturated contrast-enhanced T1WI. (C) Sagittal fat-saturated contrast-enhanced T1WI. (D) Diffusion-weighted image (DWI). (E) Apparent diffusion coefficient (ADC) map. Esthesioneuroblastoma in the right nasal cavity shows intermediate signal intensity on T2WI with heterogeneous moderate enhancement (A–C). It extends to the anterior cranial fossa and right orbit. Peritumoral cysts adjacent to the intracranial component are suggestive of esthesioneuroblastoma (arrows in A, C). The tumor shows hyperintensity to the gray matter on DWI, and the mean ADC value is  $1.345 \times 10^{-3}$  m/s.

**Box 1****Staging system for esthesioneuroblastoma***Kadish*

- A. Tumor confined to nasal cavity
- B. Tumor involved nasal cavity and paranasal sinuses
- C. Tumor spread beyond the nasal cavity and paranasal sinuses

*Modified Kadish*

- A. Tumor confined to nasal cavity
- B. Tumor involved nasal cavity and paranasal sinuses
- C. Tumor extent beyond nasal cavity and paranasal sinuses, including involvement of the cribriform plate, base of skull, orbit, or intracranial cavity
- D. Tumor with metastasis to cervical lymph nodes or distant sites

lymphoma (DLBCL) is the most common subtype. Lymphoma frequently occurs in the maxillary sinus as a discrete mass with homogeneous contrast enhancement, bone remodeling, and smooth erosion.<sup>35</sup> Due to its high cellularity, lymphoma

shows high-attenuation on CT, low-to intermediate signal intensity on T2WI, and diffusion restriction on diffusion-weighted image (DWI) (Fig. 14).

Extranodal natural killer/T-cell lymphoma (ENKTL) is the second most common subtype having a high predilection to Asians.<sup>10</sup> It often affects the nasal cavity and resembles chronic sinusitis with mucosal swelling in the early stage.<sup>14</sup> As the lesion grows, a soft tissue mass with destructive change appears in the nasal septum, resulting in septum perforation (Fig. 15). Differential diagnosis of ENKTL includes squamous cell carcinoma, granulomatosis with polyangiitis, sarcoidosis, invasive fungal sinusitis, and cocaine abuse.

Better prognosis has been reported in sinonasal DLBCL with 5-year disease-specific survival rates at 72.8% compared with ENKTL at 38.4%.<sup>10</sup>

**Melanoma** Sinonasal melanoma most often arises from the nasal septum or turbinates.<sup>14</sup> Melanoma typically presents T1WI hyperintense signal due to intratumoral hemorrhage and paramagnetic effects of melanin, although 10% to 30% of sinonasal melanomas are amelanotic and exhibit nonspecific T1WI hypointense and T2WI hyperintense signal (Fig. 16). Contrast enhancement might be difficult to observe on MR imaging for melanotic melanoma due to intrinsic T1WI

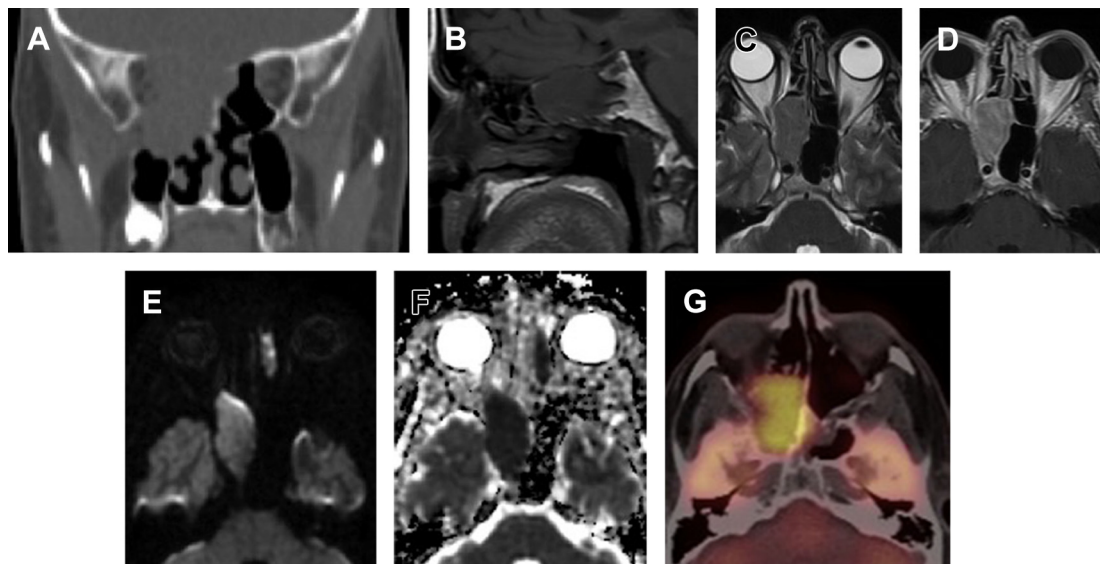


**Fig. 14.** DLBCL in the sphenoid sinus. (A) Coronal CT. (B) Sagittal T1WI. (C) Axial T2WI. (D) Axial contrast-enhanced T1WI. (E) DWI. (F) ADC map. (G) Axial FDG PET/CT. Coronal CT shows soft tissue density mass in the right sphenoid sinus involving the orbit and maxillary sinus with extensive skull base destruction (A). Subtle linear hypointense-signal on sagittal T1WI indicates the periosteum on the planum sphenoidale containing the tumor invasion (B). The tumor shows T2WI intermediate signal with moderate enhancement and marked diffusion restriction (ADC:  $457 \times 10^{-6}$  m/s), suggesting high cellularity (C–F). PET/CT demonstrates avid FDG uptake corresponded to the sphenoid lesion (G).

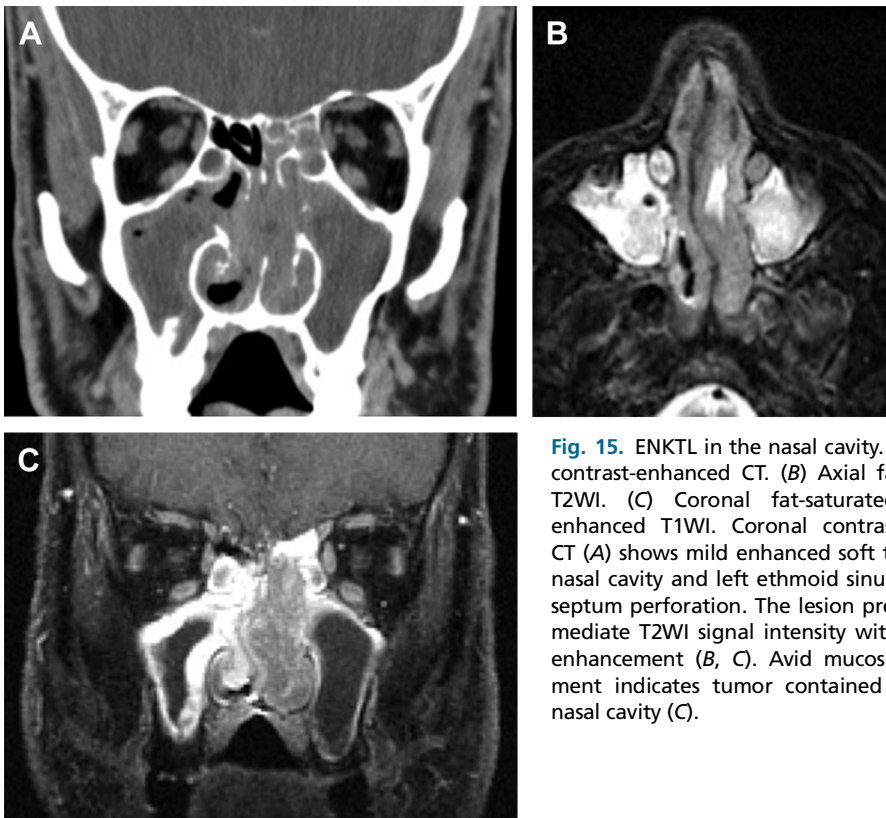


**Fig. 15.** ENKTL in the nasal cavity. (A) Coronal contrast-enhanced CT. (B) Axial fat-saturated T2WI. (C) Coronal fat-saturated contrast-enhanced T1WI. Coronal contrast-enhanced CT (A) shows mild enhanced soft tissue in the nasal cavity and left ethmoid sinus with nasal septum perforation. The lesion presents intermediate T2WI signal intensity with moderate enhancement (B, C). Avid mucosal enhancement indicates tumor contained within the nasal cavity (C).

hyperintensity. Lymph node metastasis is common (40%), and perineural extension and hematogenous metastasis are also reported.<sup>3,36</sup>

Involvement to adjacent muscle, skull base, and orbit is a negative survival predictor.<sup>37</sup> According to the 2010 AJCC staging system for mucosal melanoma of the head and neck, the mucosal disease is already considered as T3 regardless of the tumor size.<sup>12</sup> Skull base and intracranial involvement constitute a T4b disease.

Standard treatment of melanoma is surgical resection followed by radiotherapy. Chemotherapy is a treatment option for patients with metastasis or recurrence. The prognosis is poor with 5-year survival of 20% to 30%.<sup>38</sup>

#### *Sinonasal or benign neoplasm*

**Juvenile nasopharyngeal angiofibroma** Juvenile angiofibroma is a highly vascular benign tumor with a strong predilection for adolescent males. It most often arises from the sphenopalatine foramen and extends laterally to the infratemporal fossa through the pterygopalatine fissure and superiorly to the sphenoid sinus and skull base. Tumor invasion into the sphenoid bone is associated with a high risk of residual tumor

after surgery and recurrence (**Fig. 17**).<sup>39</sup> Although intracranial extension is uncommon, the middle cranial fossa is the most frequent site through the skull base foramina and fissures (**Fig. 18**). Due to its hypervasculature, it exhibits avid enhancement and signal voids within and along the periphery of the tumor (see **Fig. 18**).

Preoperative embolization is often performed to decrease intraoperative blood loss. The internal maxillary artery and the ascending pharyngeal artery are the common main feeders. In case of intracranial extension, blood supply comes from the branches of the internal carotid artery.<sup>40</sup> Transnasal endoscopic resection has become an established treatment option for relatively small juvenile angiomyxoma without intracranial extension.

**Sinonasal papilloma** Sinonasal papilloma is histopathologically classified into 3 types: inverted (62%), exophytic (32%), and oncocytic (6%) papillomas. Malignant transformation occurs in approximately 10% of inverted papillomas and 4% to 17% of oncocytic papillomas but is exceedingly rare in exophytic papillomas.<sup>41-43</sup>

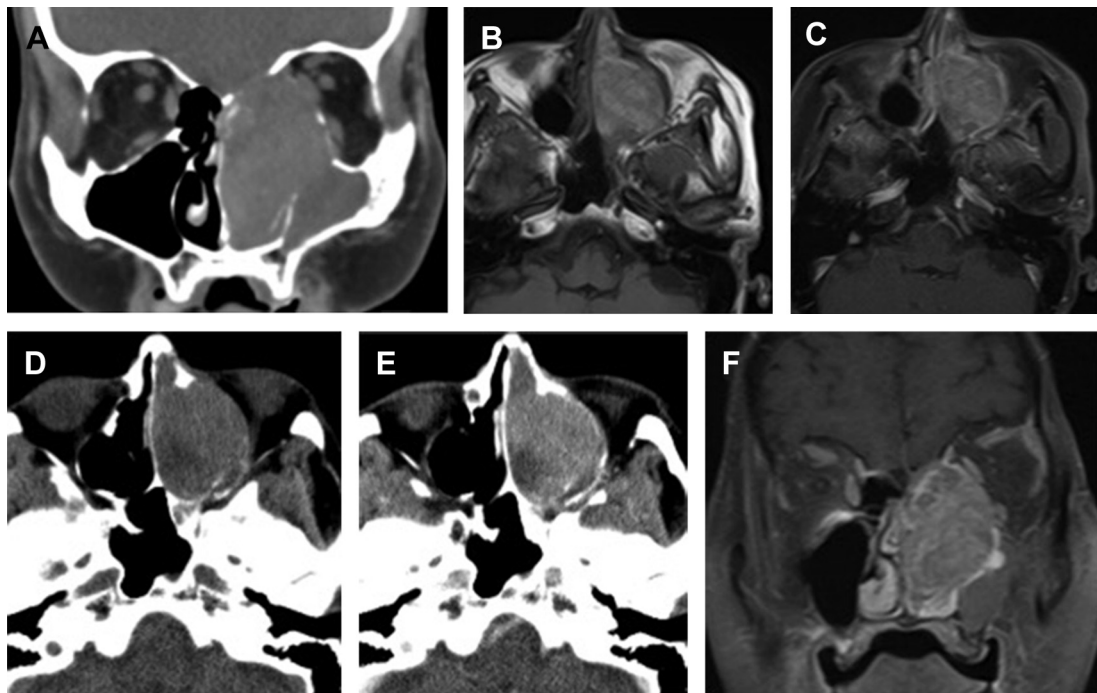


**Fig. 16.** Sinonal malignant melanoma. (A) Coronal CT. (B) Axial T1WI. (C) Axial fat-saturated contrast-enhanced T1WI. (D) Axial CT. (E) Axial contrast-enhanced CT. (F) Coronal fat-saturated contrast-enhanced T1WI. Coronal CT (A) demonstrates a large expansive tumor in the left nasal cavity with destruction of the adjacent lamina papyracea, medial orbital floor, medial maxillary wall, and cribriform plate. T1WI-hyperintense signal in the tumor is suggestive of melanotic melanoma (B). Contrast enhancement in the tumor is difficult to affirm on contrast-enhanced T1WI alone because of the intrinsic T1WI hyperintensity (C). A combination of plain and contrast-enhanced CT is useful to confirm the enhancement (D, E). Smooth bowing of the interface with the orbital contents suggests the periorbital fascia still contains the tumor infiltration.

CT usually shows a localized soft tissue mass in the early stage and extensive soft tissue opacification with bone remodeling in the advanced stage.

In inverted papilloma cases, T2WI and contrast-enhanced T1WI show a convoluted cerebriform pattern that is the combination of linear or curvilinear hyperintense and hypointense

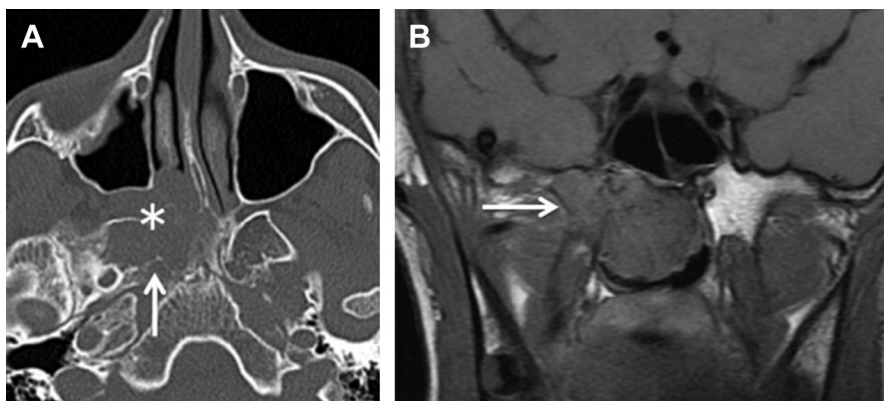


**Fig. 17.** Juvenile angiofibroma in a 14-year-old boy. (A) Axial CT. (B) Coronal T1WI. CT shows soft tissue density mass (asterisk in A) in right sphenopalatine foramen extending laterally to pterygopalatine fossa. The right pterygoid process demonstrates a lytic change on CT, and decreased signal intensity on T1WI, suggesting tumor infiltration (arrows in A, B).

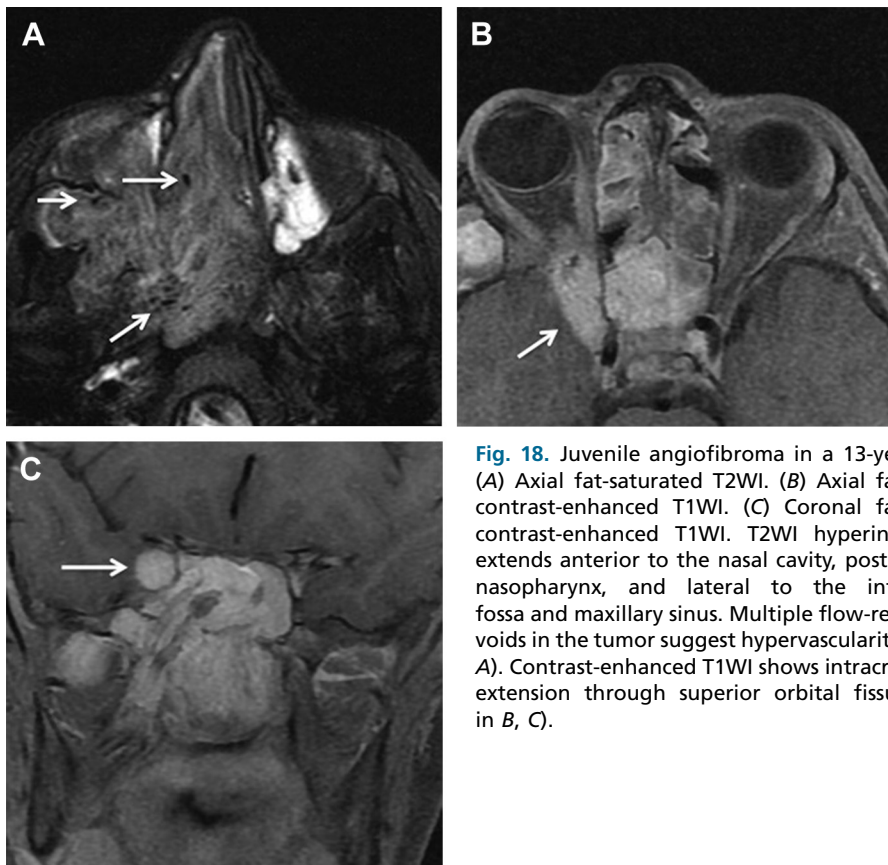


**Fig. 18.** Juvenile angiofibroma in a 13-year-old boy. (A) Axial fat-saturated T2WI. (B) Axial fat-saturated contrast-enhanced T1WI. (C) Coronal fat-saturated contrast-enhanced T1WI. T2WI hyperintense mass extends anterior to the nasal cavity, posterior to the nasopharynx, and lateral to the infratemporal fossa and maxillary sinus. Multiple flow-related signal voids in the tumor suggest hypervascularity (arrows in A). Contrast-enhanced T1WI shows intracranial tumor extension through superior orbital fissure (arrows in B, C).

striations in the solid components of the tumor (Fig. 19).<sup>44</sup>

Identification of the tumor origin is important for the complete resection because the inverted papilloma exhibits a centrifugal growth pattern.<sup>45</sup> It most often arises from the lateral nasal wall (52.6%), followed by the maxillary (25%) and anterior ethmoid sinuses (21.6%). Exophytic papillomas originate from the lower anterior nasal septum.<sup>41,45</sup> Focal hyperostosis of the sinonasal wall is a useful finding to identify its origin (see Fig. 19).<sup>45</sup>

Krouse classification (T1 to T4) is the most widely accepted staging system for inverted papilloma.<sup>46</sup> Intracranial extension is rare (1.8%) and classified as T4.<sup>47,48</sup>

The diagnosis of synchronous carcinoma is often difficult because it is distributed widely in the papilloma as multiple small foci.<sup>44,49</sup> However, presence of synchronous carcinoma is suggested when the following findings are present: extrasino-nasal extension with aggressive bone destruction, T2WI hypointense signal with loss of convoluted cerebriform pattern, intratumoral necrosis, and lymph node metastasis.<sup>44,49</sup>

Surgical excision is the treatment of choice and local recurrence is often seen in 2 to 3 years after surgery.<sup>41</sup> According to a recent study, the recurrence rate of inverted papilloma is 25.3%.<sup>43</sup>

#### Infectious disease

**Fungal rhinosinusitis** Fungal rhinosinusitis (FRS) is classified into invasive and noninvasive FRS. Invasive sinusitis includes acute (fulminant), chronic, and granulomatous, whereas noninvasive includes mycetoma and allergic FRS.

Acute invasive fungal sinusitis (AIFRS) presents a rapidly progressive course (<4 weeks), whereas chronic and granulomatous FRS have an indolent course (>4–12 weeks). Acute and chronic invasive FRS is common in immunocompromised patients and histopathologically shows fungal hyphae in the affected tissue. In contrast, granulomatous invasive FRS predominantly occurs in immunocompetent hosts, forming noncaseating granulomas with scanty fungal hyphae.

AIFRS often involves the middle turbinate as the initial site. It can rapidly extend to the orbit, skull base, and intracranial cavities. Once the intracranial contents are involved, the mortality rate is

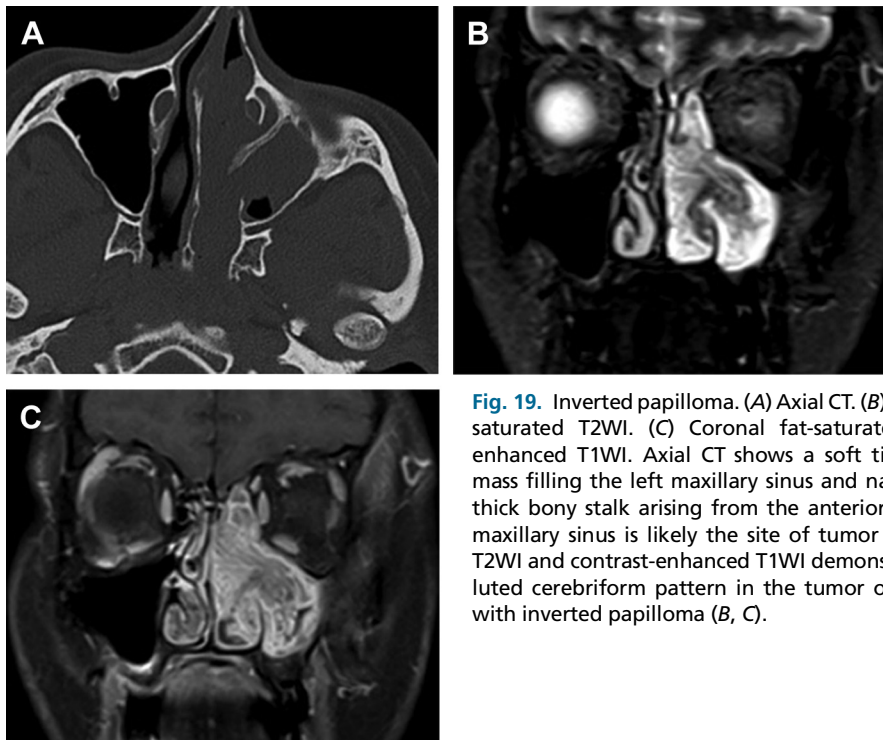


**Fig. 19.** Inverted papilloma. (A) Axial CT. (B) Coronal fat-saturated T2WI. (C) Coronal fat-saturated contrast-enhanced T1WI. Axial CT shows a soft tissue density mass filling the left maxillary sinus and nasal cavity. A thick bony stalk arising from the anterior wall of the maxillary sinus is likely the site of tumor attachment. T2WI and contrast-enhanced T1WI demonstrate convoluted cerebriform pattern in the tumor consistent with inverted papilloma (B, C).

very high. Fungal invasion of the vasculature can cause vasculitis, thrombosis, infarction, necrosis, hemorrhage, and pseudoaneurysm. Due to profound tissue necrosis, AIFRS exhibits lack of mucosal enhancement in the affected middle turbinate (Fig. 20). As the disease progresses, invasive FRS shows progressive bone destruction and extension to the orbit and the intracranial

compartment. Timely wide surgical debridement and intravenous administration of antifungals are critical for cure of invasive FRS.

#### Mucocele

Sinonasal mucoceles occur with obstruction of the sinus ostium followed by the continuous collection of mucus secretion, leading to expansile

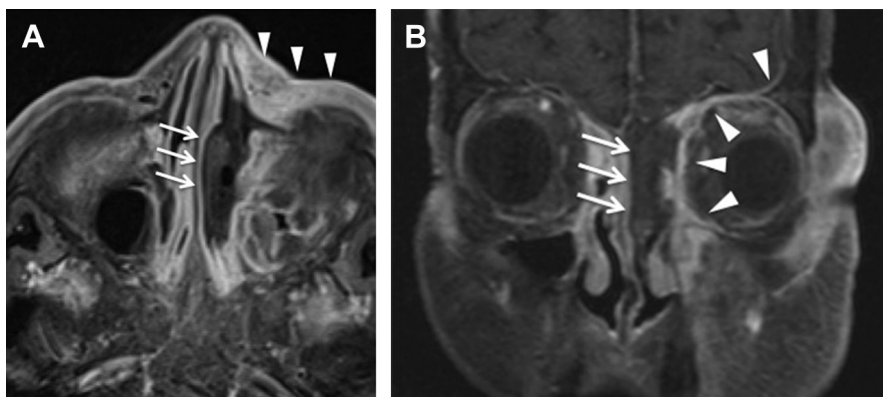


**Fig. 20.** Acute invasive fungal sinusitis in a patient with immunocompromised state presenting progressive orbital swelling. (A) Axial fat-saturated contrast-enhanced T1WI. (B) Coronal fat-saturated contrast-enhanced T1WI. Contrast-enhanced T1WIs show the lack of mucosal enhancement (arrows on A and B) of the left middle turbinate and left ethmoid sinus suggesting tissue necrosis in the setting of invasive fungal sinusitis. In contrast, left subcutaneous facial tissue shows strong enhancement with swelling, indicating inflammatory extension (arrowheads in A). Dural thickening and enhancement are also evident, as well as periorbital fascia (arrowheads in B).

remodeling of the sinus wall. The frontal sinus is the most common site for mucoceles, followed by the ethmoid, maxillary, and sphenoid sinuses in a decreasing order of frequency.<sup>50</sup> Mucoceles usually present with symptoms due to mass effect upon the adjacent structures. When a mucocele is infected symptoms include those of acute sinus infection.

CT is useful to evaluate the bony remodeling and mass effect to neighboring structures (**Fig. 21**).

MR imaging can reveal extrasinus complications, such as orbital cellulitis, meningitis, and intracranial abscess, all of which are rare occurrences.

CT attenuation and MR imaging signal intensity of mucoceles are variable depending on its protein concentration. A contrast-enhanced study shows a thin rim of contrast enhancement with no enhancement of the contents of the mucocele otherwise. Nodular or mass-like enhancement suggests neoplastic lesion with a secondary mucocele.

### Intrinsic Anterior Skull Base Lesions

#### *Osseous and fibro-osseous lesions in sinonasal cavity and anterior skull base*

The osseous and fibro-osseous lesions involving the ASB and sinonal cavities include fibrous dysplasia (FD), osteoma, ossifying fibroma, and osteoblastoma. These lesions are often asymptomatic and incidentally found. Common symptoms include headache, nasal obstruction, anosmia, and craniofacial deformity. Facial swelling and pain may occur due to chronic sinusitis, and proptosis and diplopia can be seen when the lesion extends to the orbit.

The osseous element presents bony or ground-glass attenuation and the fibrous elements present soft tissue density on CT. On MR imaging, fibro-osseous lesions may exhibit highly complex signal characteristics. The osseous parts show T1WI and T2WI hypointense signals, whereas fibrous elements demonstrate T1WI hypointensity, variable T2WI signal, and moderate to marked

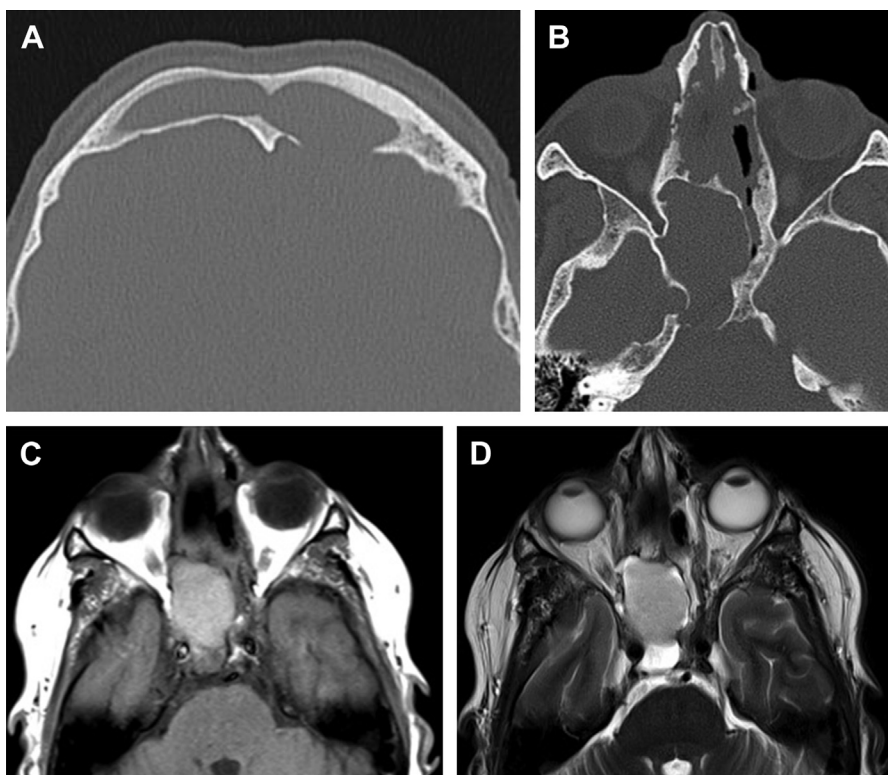


**Fig. 21.** (A) Frontal mucocele. (B–D) sphenoid mucocele. (A) Axial CT. (B) Axial CT. (C) Axial T1WI. (D) Axial T2WI. (A) Axial CT demonstrates opacification in bilateral frontal sinus with focal dehiscence at the left posterior wall. (B–D) Axial CT of another patient with a history of ethmoidectomy demonstrates expansile opacification in right sphenoid sinus with dehiscence at the posterior wall (B). Both T1WI and T2WI hyperintense signals in the sphenoid sinus suggest proteinous fluid consistent with mucocele (C, D).

contrast enhancement. T1WI hyperintensity may be present in the lesion, indicating fatty marrow.

Compressive cranial neuropathies due to involvement of neural foramina are a major indication for surgical intervention. Specifically, compression of the orbital apex and optic canal with acute or progressive visual deterioration requires immediate orbital decompression surgery. Fat-saturated T2WI and DWI may directly visualize the abnormal high signal intensity in the affected optic nerve (Fig. 22).

### Fibrous dysplasia

FD is a developmental disorder affecting the medullary bone and histologically consists of varying amounts of spindle cell bundles (fibrous tissue) and immature woven trabecular bone (osseous tissue).<sup>51,52</sup> It presents as an expansile fibro-osseous lesion with an ill-defined border to the normal medullary bone, often involving multiple craniofacial bones diffusely.

It demonstrates combinations of 3 CT attenuation patterns (ground-glass, sclerotic, and cystic), depending on the ratio of fibrous to osseous tissue (see Fig. 22). Ground-glass pattern is the typical finding, reflecting histologic findings of mixture of the fibrous and osseous tissues.<sup>51,53,54</sup>

Variable MR imaging signal patterns of FD may be mistaken for malignant neoplasms. Radiologists must consider FD in the differential diagnosis for skull base lesions and recommend additional

CT examination before biopsy, especially when the abnormal findings are incidentally found on MR imaging examinations.

### Ossifying fibroma

Ossifying fibroma is a benign fibro-osseous tumor consisting of fibrous tissue containing variable amounts of mineralized material resembling bone and cementum.<sup>55</sup> It most frequently presents in the mandible in the second decade of life with a female predominance.<sup>11,56</sup>

Sinonasal ossifying fibroma is presumed to originate from ectopic periodontal membrane and frequently occurs in the ethmoid and maxillary sinuses.<sup>57</sup> Typically, it forms an oval or spherical expansile mass with a well-defined border. The osseous elements surround the fibrous tissue (Fig. 23). Multicystic appearance with fluid-fluid levels suggests secondary aneurysmal bone cysts.<sup>11,58</sup> Tumor vascularity should be evaluated preoperatively because severe bleeding can occur during surgery.<sup>57</sup>

Endoscopic surgery is safe and effective in managing ossifying fibromas but an external approach may be necessary for tumors located in the frontal sinus or larger tumors with intracranial extension.<sup>57</sup>

### Osteoma

Osteoma is a benign lesion composed of mature bone with a predominantly lamellar structure. It

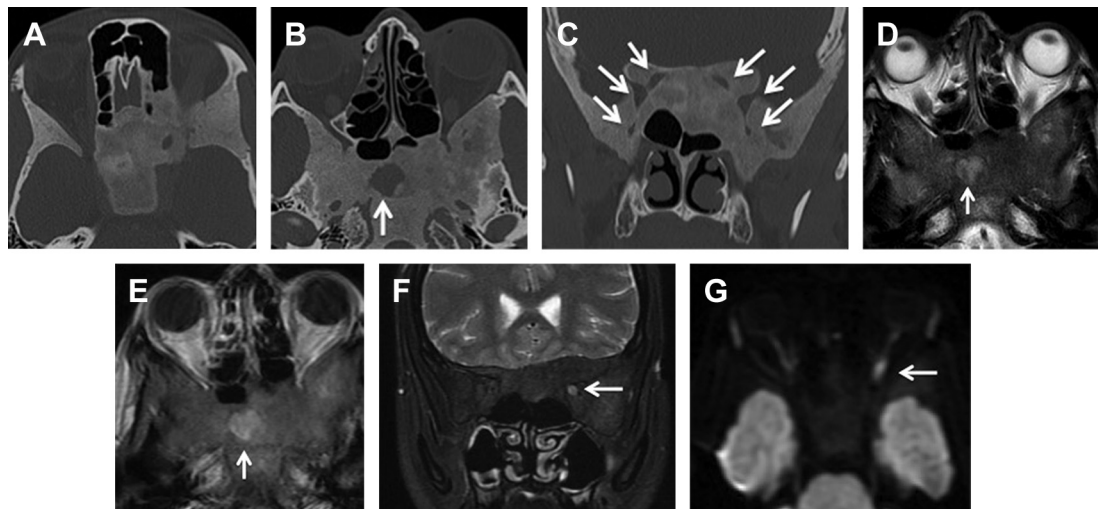


**Fig. 22.** A patient with FD (Fibrous Dysplasia) complaining of left visual disturbance. (A) Axial CT. (B) Axial. (C) Coronal CT. (D) Axial fat-saturated T2WI. (E) Axial fat-saturated contrast-enhanced T1WI. (F) Coronal fat-saturated T2WI. (G) Axial DWI. Axial and coronal CT (A–C) shows ground glass attenuated expansile lesion diffusely involving the sphenoid bones. There is severe stenosis in the optic canals, superior orbital fissures, and foramen rotundum bilaterally (arrows in C). Cystic attenuation area in the sphenoid body (arrow in B) presents T2WI hyperintensity with moderate contrast enhancement (arrow in D, E), indicating fibrous tissue. Left optic nerve (arrow in F and G) shows hyperintensity at the orbital apex on coronal T2WI and DWI, suggesting compressive neuropathy (F, G).

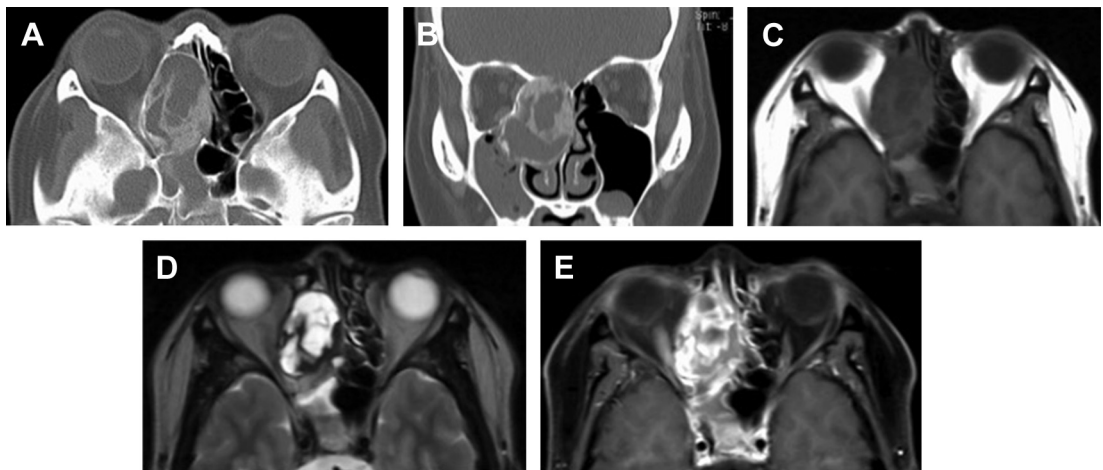


**Fig. 23.** Ossifying fibroma. (A) Axial CT. (B) Coronal CT. (C) Axial T1WI. (D) Axial T2WI. (E) Axial fat-saturated contrast-enhanced T1WI. Axial and coronal CT images demonstrate well-demarcated expansile mass involving the anterior skull base and medial orbital wall (A, B). The ossified area shows T2WI hypointensity and mild enhancement, whereas the central cystic attenuated areas show T1WI isointensity and T2WI hyperintensity and heterogeneous enhancement, indicating fibrous tissue (C–E).

occurs most commonly in the frontal and ethmoid sinuses and appears as a well-circumscribed, dense bony mass. It is generally asymptomatic though it occasionally obstructs sinus drainage pathway resulting in sinusitis or mucocele

(**Fig. 24**). If that happens, endoscopic surgery is suitable for many cases. Combined external and endoscopic approach is necessary for lesions extending lateral to a sagittal plane passing through the lamina papyracea.<sup>8,59,60</sup>

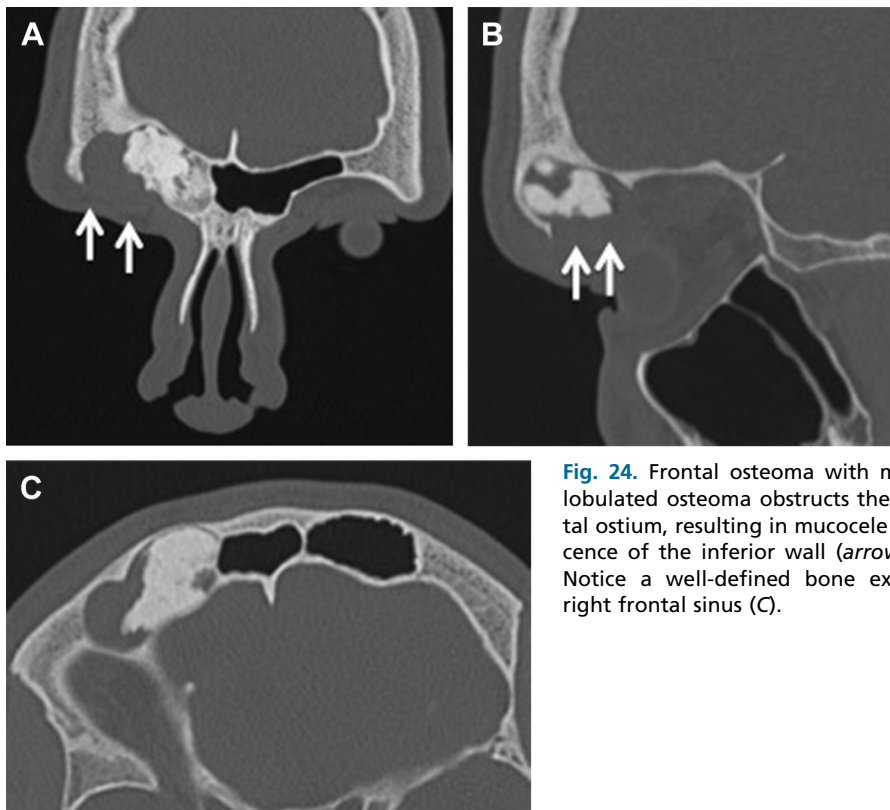


**Fig. 24.** Frontal osteoma with mucocele. A lobulated osteoma obstructs the right frontal ostium, resulting in mucocele with dehiscence of the inferior wall (arrows in A, B). Notice a well-defined bone expansion of right frontal sinus (C).

## Intracranial Lesions Involving the Anterior Skull Base

### Meningioma

ASB meningiomas are classified into olfactory groove meningioma, planum sphenoidale meningioma, or tuberculum sellae meningioma based on the site of the dural attachment (**Fig. 25**).<sup>61</sup> They appear as well-circumscribed, smooth, or lobulated lesions. Dural thickening, known as the dural tail sign, is suggestive of meningioma, although it may be present in other neoplastic and non-neoplastic lesions.<sup>62</sup> Hyperostosis is often present in the adjacent bone. CT demonstrates isoattenuating to hyperattenuating mass. Intratumoral calcifications may be present. On MR imaging, the tumor shows isointense signal to the cortex on T1WI and T2WI. Peritumoral edema can present in variable degrees. Imaging plays a significant role in evaluating the extent of the ASB meningioma and in determining the optimal surgical approach and reconstruction procedure. Complete resection may be difficult if the tumor involves vital structures, such as the cavernous sinuses and optic nerves, or encases the anterior cerebral arteries or internal carotid arteries.<sup>63</sup>

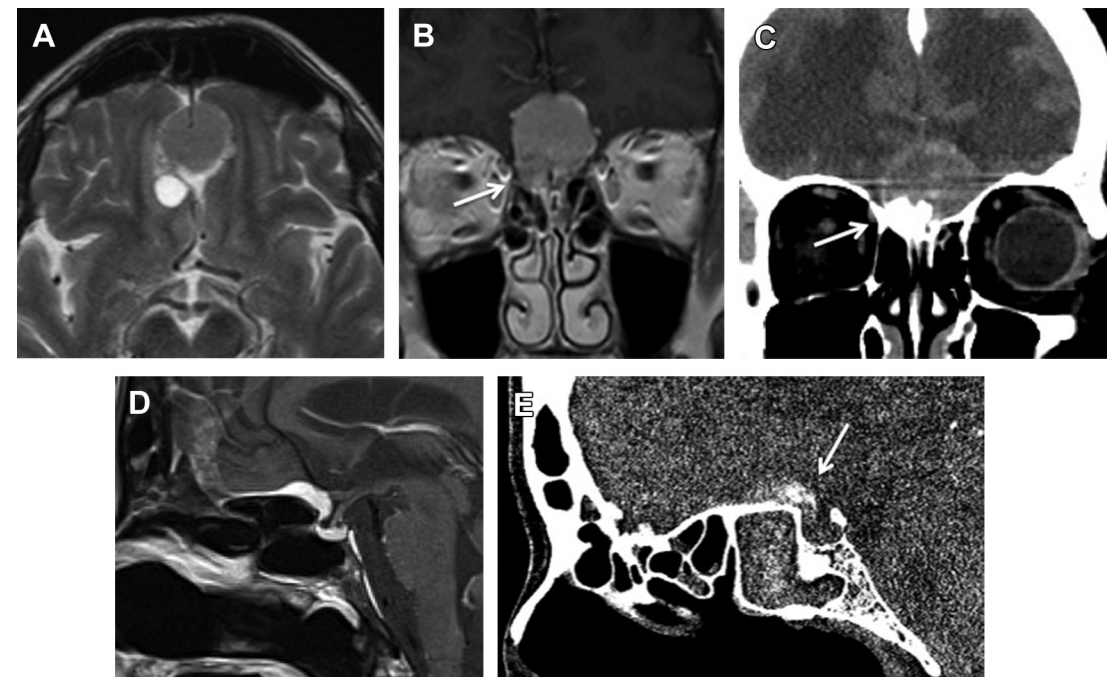


**Fig. 25.** (A–C) Olfactory groove meningioma. (D, E) Tuberculum sellae meningioma. (A) Axial T2WI. (B) Coronal contrast-enhanced T1WI. (C) Coronal CT. (D) Sagittal contrast-enhanced T1WI. (E) Sagittal CT. (A–C) Axial T2WI shows a lesion in the olfactory groove with a peritumoral cyst. Homogeneous enhancing tumor involves the right upper nasal vault through the cribriform plate with hyperostosis (arrows in B, C). (D, E) Sagittal contrast-enhanced T1WI shows a small tuberculum sellae meningioma with adjacent dura thickening (D). Sagittal CT image shows calcification (arrow in E) in the lesion (E).

### Nasal cephalocele

Cephalocele is a congenital or acquired herniation of intracranial contents through a skull defect and divided into encephalocele and meningocele. Whereas encephalocele contains brain tissue, meninges, and CSF, meningocele contains meninges and CSF only without brain tissue in its content. The frontoethmoidal (sincipital) and basal cephaloceles are associated with ASB and sино-nasal cavity.

CT can demonstrate the extent of skull base defect (**Fig. 26**). MR imaging is suitable for determination of herniated content. Because the skull base ossification is not yet complete in infants, CT may overestimate the size of the bone defect.<sup>14</sup> Most of the ASB is completely ossified by 24 months.<sup>64</sup> Encephalocele contains (see **Fig. 26**) a herniated brain tissue, which is isointense to brain parenchyma. MR imaging allows a close inspection of the herniated contents in pre-operative evaluation. Particularly, basal encephaloceles can contain critical structures, such as pituitary gland and hypothalamus, olfactory nerve, optic pathways, and branches of the anterior cerebral artery.

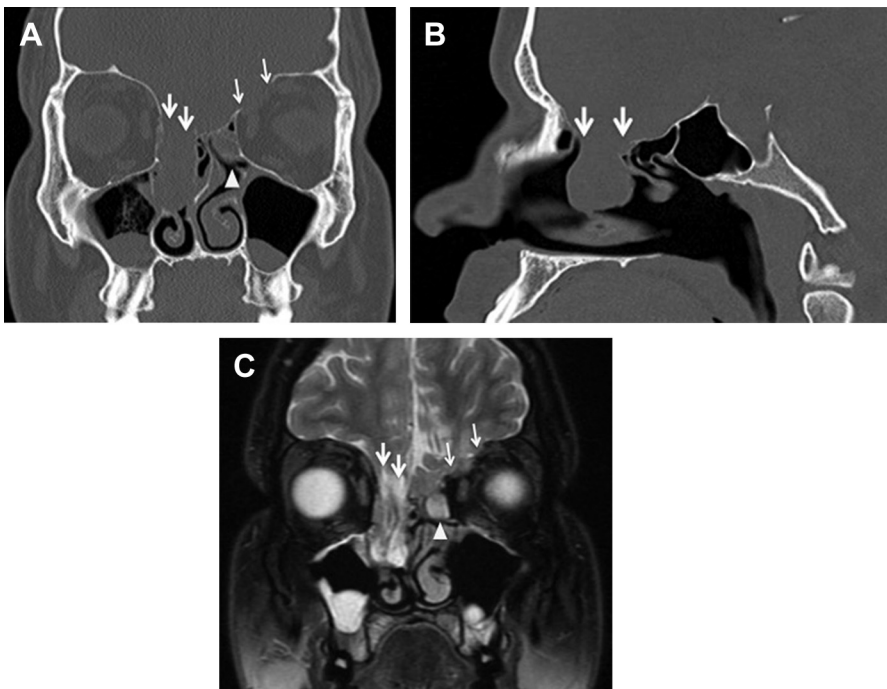


**Fig. 26.** Tranethmoid encephalocele. (A) Coronal CT. (B) Sagittal CT. (C) Coronal fat-saturated T2WI. Coronal and sagittal CT images show the bone defect in the right ethmoid roof (large arrows in A and C) and the left orbital plate (small arrows in A). Soft tissue density masses fill the right ethmoid sinus and upper nasal cavity. Coronal T2WI demonstrates a mixed intensity mass with a direct connection to intracranial space, confirming the right tranethmoidal encephalocele. Left frontal parenchyma slightly protrudes into left orbit through the dehiscence of the left orbital plate. A cystic lesion (arrowheads in A, C) in the left ethmoid cell is another tranethmoidal encephalocele (the connection with an intracranial cavity is not demonstrated in the figures).

## SUMMARY

The ASB has a close relation to the sinonasal cavity. In addition to the intrinsic ASB lesions, sinonasal and intracranial diseases extend inferiorly to involve the ASB. CT and MR imaging play a complementary role in evaluating the ASB pathologic conditions. Radiologists should be familiar with the detailed anatomy, identify dangerous anatomic variations, provide appropriate differential diagnosis, and assess the extent of the lesion for optimal treatment planning.

## REFERENCES

- Keros P. Über die praktische Bedeutung der Niveauunterschiede der Lamina cribrosa des Ethmoids. *Z Laryngol Rhinol Otol* 1962;41: 808–13.
- García-Garrigós E, Arenas-Jiménez JJ, Monjas-Cánovas I, et al. Transsphenoidal approach in endoscopic endonasal surgery for skull base lesions: what radiologists and surgeons need to know. *Radiographics* 2015;35(4):1170–85.
- Mossa-Basha M, Blitz AM. Imaging of the paranasal sinuses. *Semin Roentgenol* 2013;48(1):14–34.
- Hoang JK, Eastwood JD, Tebbit CL, et al. Multiplanar sinus CT: a systematic approach to imaging before functional endoscopic sinus surgery. *AJR Am J Roentgenol* 2010;194(6):W527–36.
- Nouraei SA, Elisay AR, Dimarco A, et al. Variations in paranasal sinus anatomy: implications for the pathophysiology of chronic rhinosinusitis and safety of endoscopic sinus surgery. *J Otolaryngol Head Neck Surg* 2009;38(1):32–7.
- Shpilberg KA, Daniel SC, Doshi AH, et al. CT of anatomic variants of the paranasal sinuses and nasal cavity: poor correlation with radiologically significant rhinosinusitis but importance in surgical planning. *AJR Am J Roentgenol* 2015; 204(6):1255–60.
- Beale TJ, Madani G, Morley SJ. Imaging of the paranasal sinuses and nasal cavity: normal anatomy and clinically relevant anatomical variants. *Semin Ultrasound CT MR* 2009;30(1):2–16.
- Turri-Zanoni M, Dallan I, Terranova P, et al. Fronoothmoidal and intraorbital osteomas: exploring the limits of the endoscopic approach. *Arch Otolaryngol Head Neck Surg* 2012;138(5):498–504.

9. Barnes L, Eveson JW, Reichart P, et al. World Health Organization classification of tumours. Pathology and genetics of head and neck tumours. Lyon (France): IARC; 2005. p. 210–81.
10. Dubal PM, Dutta R, Vazquez A, et al. A comparative population-based analysis of sinonasal diffuse large B-cell and extranodal NK/T-cell lymphomas. *Laryngoscope* 2015;125(5):1077–83.
11. Kendi AT, Kara S, Altinok D, et al. Sinonasal ossifying fibroma with fluid-fluid levels on MR images. *AJNR Am J Neuroradiol* 2003;24(8):1639–41.
12. Edge S, Byrd D, Compton C, et al. AJCC Cancer Staging Manual. 7th edition. New York: Springer-Verlag; 2010.
13. Connor SEJ. The skull base in the evaluation of sino-nasal disease: role of computed tomography and MR imaging. *Neuroimaging Clin N Am* 2015;25(4): 619–51.
14. Parmar H, Gujar S, Shah G, et al. Imaging of the anterior skull base. *Neuroimaging Clin N Am* 2009; 19(3):427–39.
15. Maroldi R, Ravanelli M, Borghesi A, et al. Paranasal sinus imaging. *Eur J Radiol* 2008;66(3):372–86.
16. Eisen MD, Yousem DM, Montone KT, et al. Use of preoperative MR to predict dural, perineural, and venous sinus invasion of skull base tumors. *AJNR Am J Neuroradiol* 1996;17(10):1937–45.
17. Gallagher KK, Spector ME, Pepper JP, et al. Esthesioneuroblastoma: updating histologic grading as it relates to prognosis. *Ann Otol Rhinol Laryngol* 2014;123(5):353–8.
18. Som PM, Lidov M, Brandwein M, et al. Sinonasal esthesioneuroblastoma with intracranial extension: marginal tumor cysts as a diagnostic MR finding. *AJNR Am J Neuroradiol* 1994;15(7):1259–62.
19. Yu T, Xu YK, Li L, et al. Esthesioneuroblastoma methods of intracranial extension: CT and MR imaging findings. *Neuroradiology* 2009;51(12): 841–50.
20. Pickuth D, Heywang-Kobrunner SH, Spielmann RP. Computed tomography and magnetic resonance imaging features of olfactory neuroblastoma: an analysis of 22 cases. *Clin Otolaryngol Allied Sci* 1999;24(5):457–61.
21. Tajudeen BA, Arshi A, Suh JD, et al. Esthesioneuroblastoma: an update on the UCLA experience, 2002–2013. *J Neurol Surg B Skull Base* 2015; 76(1):43–9.
22. Patel SG, Singh B, Stambuk HE, et al. Craniofacial surgery for esthesioneuroblastoma: report of an international collaborative study. *J Neurol Surg B Skull Base* 2012;73(3):208–20.
23. Dulguerov P, Calcaterra T. Esthesioneuroblastoma: the UCLA experience 1970–1990. *Laryngoscope* 1992;102(8):843–9.
24. Petruzzelli GJ, Howell JB, Pederson A, et al. Multi-disciplinary treatment of olfactory neuroblastoma: patterns of failure and management of recurrence. *Am J Otolaryngol* 2015;36(4):547–53.
25. Snyderman CH, Carrau RL, Kassam AB, et al. Endoscopic skull base surgery: principles of endonasal oncological surgery. *J Surg Oncol* 2008;97(8):658–64.
26. Kadish S, Goodman M, Wang CC. Olfactory neuroblastoma. A clinical analysis of 17 cases. *Cancer* 1976;37(3):1571–6.
27. Morita A, Ebersold MJ, Olsen KD, et al. Esthesioneuroblastoma: prognosis and management. *Neurosurgery* 1993;32(5):706–14 [discussion: 714–5].
28. Feng L, Fang J, Zhang L, et al. Endoscopic endonasal resection of esthesioneuroblastoma: a single center experience of 24 patients. *Clin Neurol Neurosurg* 2015;138:94–8.
29. Van Gompel JJ, Giannini C, Olsen KD, et al. Long-term outcome of esthesioneuroblastoma: hyams grade predicts patient survival. *J Neurol Surg B Skull Base* 2012;73(5):331–6.
30. Song CM, Won TB, Lee CH, et al. Treatment modalities and outcomes of olfactory neuroblastoma. *Laryngoscope* 2012;122(11):2389–95.
31. Ozsahin M, Gruber G, Olszyk O, et al. Outcome and prognostic factors in olfactory neuroblastoma: a rare cancer network study. *Int J Radiat Oncol Biol Phys* 2010;78(4):992–7.
32. Kane AJ, Sughrue ME, Rutkowski MJ, et al. Post-treatment prognosis of patients with esthesioneuroblastoma. *J Neurosurg* 2010;113(2):340–51.
33. Dulguerov P, Allal AS, Calcaterra TC. Esthesioneuroblastoma: a meta-analysis and review. *Lancet Oncol* 2001;2(11):683–90.
34. Rinaldo A, Ferlito A, Shaha AR, et al. Esthesioneuroblastoma and cervical lymph node metastases: clinical and therapeutic implications. *Acta Otolaryngol* 2002;122(2):215–21.
35. Peng KA, Kita AE, Suh JD, et al. Sinonasal lymphoma: case series and review of the literature. *Int Forum Allergy Rhinol* 2014;4(8):670–4.
36. Chang PC, Fischbein NJ, McCalmon TH, et al. Perineural spread of malignant melanoma of the head and neck: clinical and imaging features. *AJNR Am J Neuroradiol* 2004;25(1):5–11.
37. Roth TN, Gengler C, Huber GF, et al. Outcome of sinonasal melanoma: clinical experience and review of the literature. *Head Neck* 2010;32(10):1385–92.
38. Khan MN, Kanumuri VV, Raikundalia MD, et al. Sinonasal melanoma: survival and prognostic implications based on site of involvement. *Int Forum Allergy Rhinol* 2014;4(2):151–5.
39. Boghani Z, Husain Q, Kanumuri VV, et al. Juvenile nasopharyngeal angiofibroma: a systematic review and comparison of endoscopic, endoscopic-assisted, and open resection in 1047 cases. *Laryngoscope* 2013;123(4):859–69.
40. Ballah D, Rabinowitz D, Vossough A, et al. Preoperative angiography and external carotid artery

- embolization of juvenile nasopharyngeal angiofibromas in a tertiary referral paediatric centre. *Clin Radiol* 2013;68(11):1097–106.
41. Barnes L, Tse LLY, Hunt JL, et al. Tumours of the nasal cavity and paranasal sinuses. Pathology and Genetics of Head and Neck Tumors. Proceeding of IARC (International Agency for Research on Cancer) Press Lyon, France, July 13–16, 2003.
  42. von Buchwald C, Bradley PJ. Risks of malignancy in inverted papilloma of the nose and paranasal sinuses. *Curr Opin Otolaryngol Head Neck Surg* 2007;15(2):95–8.
  43. Nygren A, Kiss K, Von Buchwald C, et al. Rate of recurrence and malignant transformation in 88 cases with inverted papilloma between 1998–2008. *Acta Otolaryngol* 2016;136(3):333–6.
  44. Jeon TY, Kim HJ, Chung SK, et al. Sinonasal inverted papilloma: value of convoluted cerebriform pattern on MR imaging. *AJNR Am J Neuroradiol* 2008;29(8):1556–60.
  45. Lee DK, Chung SK, Dhong HJ, et al. Focal hyperostosis on CT of sinonasal inverted papilloma as a predictor of tumor origin. *AJNR Am J Neuroradiol* 2007; 28(4):618–21.
  46. Krouse JH. Development of a staging system for inverted papilloma. *Laryngoscope* 2000;110(6): 965–8.
  47. Lawson W, Ho BT, Shaari CM, et al. Inverted papilloma: a report of 112 cases. *Laryngoscope* 1995; 105(3):282–8.
  48. Mohan S, Nair S, Sharma M, et al. Inverted papilloma of frontal sinus with intracranial extension. *Med J Armed Forces India* 2015;71:S152–5.
  49. Ojiri H, Ujita M, Tada S, et al. Potentially distinctive features of sinonasal inverted papilloma on MR imaging. *AJR Am J Roentgenol* 2000;175(2):465–8.
  50. Capra GG, Carbone PN, Mullin DP. Paranasal sinus mucocele. *Head Neck Pathol* 2012;6(3):369–72.
  51. Brown EW, Megerian CA, McKenna MJ, et al. Fibrous dysplasia of the temporal bone: Imaging findings. *AJR Am J Roentgenol* 1995;164(3):679–82.
  52. Kransdorf MJ, Moser RP Jr, Gilkey FW. Fibrous dysplasia. *Radiographics* 1990;10(3):519–37.
  53. Fries JW. The roentgen features of fibrous dysplasia of the skull and facial bones; a critical analysis of thirty-nine pathologically proved cases. *Am J Roentgenol Radium Ther Nucl Med* 1957; 77(1):71–88.
  54. Chong VFH, Khoo JBK, Fan YF. Fibrous dysplasia involving the base of the skull. *AJR Am J Roentgenol* 2002;178(3):717–20.
  55. Urs AB, Kumar P, Arora S, et al. Clinicopathologic and radiologic correlation of ossifying fibroma and juvenile ossifying fibroma - An institutional study of 22 cases. *Ann Diagn Pathol* 2013;17(2): 198–203.
  56. Manes RP, Ryan MW, Batra PS, et al. Ossifying fibroma of the nose and paranasal sinuses. *Int Forum Allergy Rhinol* 2013;3(2):161–8.
  57. Wang H, Sun X, Liu Q, et al. Endoscopic resection of sinonasal ossifying fibroma: 31 cases report at an institution. *Eur Arch Otorhinolaryngol* 2014;271(11): 2975–82.
  58. Yang BT, Wang YZ, Wang XY, et al. Imaging study of ossifying fibroma with associated aneurysmal bone cyst in the paranasal sinus. *Eur J Radiol* 2012; 81(11):3450–5.
  59. Schick B, Steigerwald C, El Tahan AER, et al. The role of endonasal surgery in the management of frontoethmoidal osteomas. *Rhinology* 2001;39(2): 66–70.
  60. Karligkiotis A, Pistochini A, Turri-Zanoni M, et al. Endoscopic endonasal orbital transposition to expand the frontal sinus approaches. *Am J Rhinol Allergy* 2015;29(6):449–56.
  61. Refaat MI, Eissa EM, Ali MH. Surgical management of midline anterior skull base meningiomas: experience of 30 cases. *Turk Neurosurg* 2015; 25(3):432–7.
  62. Wallace EW. The dural tail sign. *Radiology* 2004; 233(1):56–7.
  63. Shin M, Kondo K, Saito N. Current status of endoscopic endonasal surgery for skull base meningiomas: review of the literature. *Neurol Med Chir (Tokyo)* 2015;55(9):735–43.
  64. Belden CJ, Mancuso AA, Kotzur IM. The developing anterior skull base: CT appearance from birth to 2 years of age. *AJNR Am J Neuroradiol* 1997;18(5): 811–8.